The Journal of Physical Chemistry Letters

Letter

pubs.acs.org/JPCL

Potential Dependence of Surfactant Adsorption at the Graphite Electrode/Deep Eutectic Solvent Interface

Katharina Häckl,[†,‡] Hua Li,[‡] Iain Aldous,[§] Terrence Tsui,[‡] Werner Kunz,[†] Andrew P. Abbott,[§] Gregory G. Warr,[∥] and Rob Atkin*[,‡]

[†]Institute of Physical and Theoretical Chemistry, University of Regensburg, Universitätsstraße 31, D-93053 Regensburg, Germany

[‡]School of Molecular Sciences, The University of Western Australia, 35 Stirling Highway, Perth, WA 6009, Australia

[§]Materials Centre, Department of Chemistry, University of Leicester, Leicester LE1 7RH, U.K.

[∥]School of Chemistry and University of Sydney Nano Institute, The University of Sydney, Camperdown, NSW 2006, Australia

Supporting Information

ABSTRACT: Atomic force microscope and cyclic voltammetry are used to probe how ionic surfactant adsorbed layer structure affects redox processes at deep eutectic solvent (DES)/graphite interfaces. Unlike its behavior in water, sodium dodecyl sulfate (SDS) in DESs only adsorbs as a complete layer of hemicylindrical hemimicelles far above its critical micelle concentration (CMC). Near the CMC it forms a tail-to-tail monolayer at open-circuit potential (OCP) and positive potentials, and it desorbs at negative potentials. In contrast, cetyltrimethylammonium bromide (CTAB) adsorbs as hemimicelles at low concentrations and remains adsorbed at both positive and negative potentials. The SDS horizontal monolayer has little overall effect on redox processes at the graphite interface, but hemimicelles form an effective and stable barrier. The stronger solvophobic interactions between the C_{16} versus C_{12} alkyl chains in the DES allow CTAB to self-assemble into a robust coating at low concentrations and illustrate how the structure of the DES/electrode interface and electrochemical response can be engineered by controlling surfactant structure.

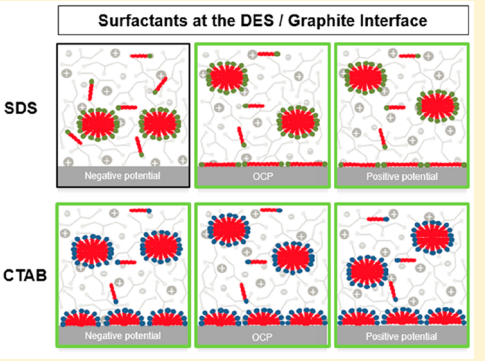

Deep eutectic solvents (DESs) are a promising new solvent class prepared by simply mixing an organic salt with a molecular hydrogen-bond donor (HBD). Properties comparable to ionic liquids (ILs) and large melting point depressions of the individual components are realized by exploiting strong H-bond interactions between the components in order to stabilize the liquid state, but with the advantage of utilizing a wide range of inexpensive, environmentally benign constituents. DESs are exemplified by a 1:2 mole:mole mixture of choline chloride (mp 302 °C) and urea (mp 132 °C), which has a melting point below 30 °C and even lower in the presence of small amounts of water.[1,2] Other widely examined DESs use glycerol or ethylene glycol as the HBD. The DES cation has low symmetry but, like the molecular component, the ability to form a range of hydrogen bonds. This wide variety of possible interactions between the liquid constituents produces a high entropy state and low melting points at the eutectic composition.[3−6]

Like ILs, DESs have high ionic strength, low volatility, nonflammability, and high thermal stability and can be viewed as designer solvents because of the wide range of potential ionic and HBD constituents. DES research is currently focused in six main areas: electrochemistry, material preparation, synthesis, catalysis, separations, and bioapplications. DESs have been used for electrodeposition, electropolishing, and electrolyte preparation[7−15] and to produce well-defined nanoparticles,[16,17] metal−organic frameworks,[18,19] porous nanocarbons,[20,21] and colloidal materials.[22] The extensive exploration of the use of DESs in electrochemical applications is a consequence of many having a wide electrochemical window. In this context, a deep understanding of the DES liquid nanostructure at electrode interfaces is critical for optimizing electrochemical processes. While the liquid nanostructure of ILs at solid interfaces has attracted much research interest,[23−32] to date only a few studies of the double-layer structure of DESs have been reported. Our group has used atomic force microscopy (AFM) force−distance curves to probe the structure of DESs at solid and electrode interfaces. Hammond et al. and Chen et al. examined the formation of layered, molecularly segregated DES nanostructures at platinum and graphite interfaces as a function of surface potential.[33−35] At both interfaces a counterion-rich Stern layer was found in contact with the electrode, followed by a second layer rich in molecular HBD component. For Pt electrodes, the interfacial nanostructure extended further into the bulk DES upon water addition up to ∼40 wt %. This is surprising, as

Received: July 8, 2019
Accepted: August 20, 2019
Published: August 20, 2019

DOI: 10.1021/acs.jpclett.9b01968
J. Phys. Chem. Lett. XXXX, XXX, XXX−XXX

generally addition of even small amounts of water diminishes liquid nanostructure at IL interfaces.[36−38]

Recent studies have investigated methods of controlling the morphology of electrodeposited films by optimizing conditions and adding brighteners and levellers.[39−43] Surfactants are commonly employed in conventional electrochemical systems to widen electrochemical windows, control the crystal size of deposited metals, and reduce the surface tension of electroplating solutions to facilitate bubble detachment and prevent pitting.[44] Two studies investigating the use of anionic and cationic surfactants for the electrodeposition of Zn and Ag in DESs found that surfactants had negligible effect on deposition rates and only minor changes in morphology.[45,46] Conversely, compounds known to specifically interact with the surface had a more marked effect on deposit morphology.[47] Surfactant adsorption at solid/liquid interfaces depends on the relative magnitude of solvent−surface, solvent−surfactant, surface−surfactant, and surfactant−surfactant interactions. In aqueous systems, oppositely charged surfactants adsorb and form admicelles or bilayers on hydrophilic surfaces, but on hydrophobic surfaces like graphite, surfactant alkyl chain−surface interactions dominate, and hemimicelles form.[48] In both cases, the resulting interfacial aggregates can be imaged in situ using AFM.[49−55] Similar hemimicellar structures have been reported in nonaqueous solvents, including formamide[56] and the protic ionic liquid ethylammonium nitrate.[54] To date, surfactant adsorption at DES/solid interfaces has not been studied.

Here we investigate the adsorbed layer structure of sodium dodecyl sulfate (SDS) and cetyltrimethylammonium bromide (CTAB) at DES−graphite electrode interfaces using AFM soft-contact imaging and cyclic voltammetry (CV). The effect of the DES type, surfactant concentration, and surface potential is probed. Details of the DES preparation and the AFM and CV experiments, are provided in the Supporting Information.

Previously reported CMCs for CTAB in 1:2 choline chloride:ethylene glycol (ChCl-EG), and SDS in ChCl-EG and 1:2 choline chloride:glycerol (ChCl-Gly), are presented in Table 1, alongside their values in water.[48] The CMC of SDS in ChCl-EG is 9 mM, almost the same as in water, but the CMC for SDS in ChCl-Gly is much reduced to 3.8 mM.[57] The CTAB CMC in ChCl-Gly is 1 mM,[58] essentially the same as its aqueous value of 0.9 mM.[59] In water, surfactant aggregation on surfaces usually begins at concentrations from 0.5−0.8 × CMC. In order to provide the best chance of detecting aggregates adsorbed at the DES/graphite interface, we investigated a variety of concentrations greater than the CMC.

Table 1. Literature CMC (mM) Values for SDS and CTAB in ChCl-EG, ChCl-Gly, and Water at 25 °C

	ChCl-EG (mM)	ChCl-Gly (mM)	water (mM)
SDS	9.0[57]	3.8[57]	8.2[60]
CTAB	insoluble	<1[58,a]	0.9[59]

[a]In ref 61 the authors incorrectly report a CMC value of ∼15 mM. Examination of the fluorescence, conductivity, and surface tension data in the article conclusively shows the CMC is, at most, 1 mM.

Figure 1 presents soft contact AFM images for 25 and 132 mM SDS at the ChCl-EG/graphite interface and for 21 mM SDS and 2.5 mM CTAB at the ChCl-Gly/graphite interface. The images consist of straight parallel stripes like those found for SDS and CTAB in water.[49−53,55] This means that at open-circuit potential (OCP), where the graphite is negatively charged,[34] both cationic and anionic surfactants displace the strongly bound choline cation from the surface in order to achieve such a highly ordered adsorbed layer structure.

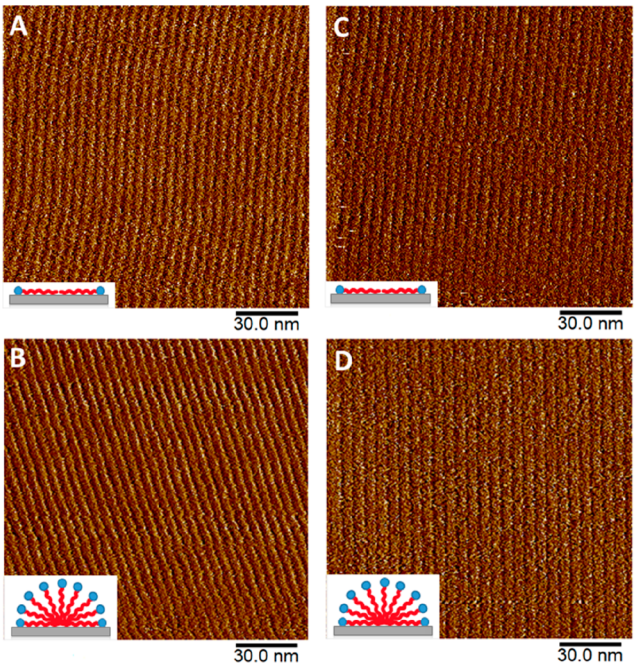

Figure 1. AFM deflection images for the (A) 25 mM and (B) 132 mM SDS at the graphite/ChCl-EG interface, (C) 21 mM SDS at the graphite/ChCl-Gly interface, and (D) 2.5 mM CTAB at the graphite/ChCl-Gly interface. The deflection height scales are (A) 0.3 nm, (B) 1 nm, (C) 0.5 nm, and (D) 1 nm. The image insets show the adsorbed surfactant structure in each system: (A and C) a tail-to-tail horizontal monolayer and (B and D) a fully formed hemimicelle.

In aqueous solution, surfactants first adsorb onto graphite with their alkyl tails parallel with the surface, in a tail-to-tail arrangement, producing a horizontal monolayer at concentrations around 0.1 × CMC. These tails are epitaxially aligned along one of the three graphite symmetry axes. Flat epitaxial adsorption is ascribed to a precise match between surfactant alkyl chain hydrogen atoms and the hexagon centers of the graphene lattice.[62] As the surfactant concentration approaches the CMC, hydrophobic interactions lead to additional surfactant adsorption leading to the formation of hemicylindrical hemimicelles, templated by the strongly adsorbed monolayer. The image deflection height can be used to discern whether the stripes are due to a tail-to-tail monolayer or hemicylinders, as deflections are significantly higher for the larger hemicylinder structures.

The striking similarity between the images obtained in this work and aqueous systems implies that the same adsorption mechanism operates for surfactants in these DESs. The small deflection height of 0.3 nm for 25 mM SDS in ChCl-EG shows the surfactant to be adsorbed as a tail-to-tail monolayer, whereas the much larger deflection at 132 mM SDS reveals them to have developed into hemicylinders (Figure 1, insets). This is similar to the evolution of adsorbed layer structure with concentration of SDS at the graphite/water interface[51] and of surfactants adsorbed at the graphite/ethylammonium nitrate interface.[54] SDS in ChCl-Gly also forms a monolayer at 21 mM, which is near its solubility limit and prevents study of higher concentrations. In contrast, CTAB exhibits larger

DOI: 10.1021/acs.jpclett.9b01968
J. Phys. Chem. Lett. XXXX, XXX, XXX−XXX

Table 2. Concentration (mM), Structure Type (Tail-to-Tail *Monolayer* or *Hemimicelle*), and Structure Period (nm ± 0.1 nm) Determined from AFM Images

	ChCl-EG			ChCl-Gly			water		
	conc. (mM)	structure	period (nm)	conc. (mM)	structure	period (nm)	conc. (mM)	structure	period (nm)
SDS	25	monolayer	5.0	21	monolayer	5.2	2.8	hemimicelle	7[51]
	132	hemimicelle	5.0	>21	*insoluble*		>20	hemimicelle	5.3[51]
CTAB		*insoluble*		2.5	hemimicelle	5.5	1.8	hemimicelle	9.1[52]
				21	hemimicelle	5.5	5	hemimicelle	4.2[49,a]

[a]Hemimicelles were not aligned parallel to the scan direction in the image used to calculate this value; therefore, it is likely less than the true aggregate spacing.

deflections and forms hemimicelles at concentrations as low as 2.5 mM in ChCl-Gly. This reflects the much stronger tendency for CTAB to self-assemble due to its longer alkyl tail.

The period of the stripes captures the aggregate size plus the interaggregate separation, which results from repulsions between adsorbed surfactant headgroups. Aggregate periods were determined via power spectral density analysis of images with aggregates aligned not more than ±5° from perpendicular (the slow scan direction) as this provides the most accurate values. Table 2 shows aggregate periods for the systems investigated here, together with literature values. For 25 mM and 132 mM SDS solutions, the period was identical at 5.0 ± 0.1 nm, indicating that the hemicylinders assemble over the underlying tail-to-tail monolayer. This spacing is similar to that of SDS in water for concentrations greater than 20 mM.[51]

In ChCl-Gly, the SDS stripes have a similar period (5.2 ± 0.1 nm) and small imaging deflection range at 21 mM, also consistent with a tail-to-tail monolayer. The CTAB stripe period is also constant at 5.5 ± 0.1 nm as concentration is increased from 2.5 to 21 mM in ChCl-Gly (Table 2). This differs from reported behavior in water, where the hemimicelle period decreases with increasing surfactant concentration, or upon addition of salt. The periodicity of ∼7 nm for 2.8 mM SDS decreased to ∼5.3 nm at concentrations >20 mM.[51] Similarly, for CTAB the period decreased from 9.1 nm at 1.8 mM to 4.2 nm at 5 mM in water.[49,52] (Note the hemimicelles were not aligned parallel to the scan direction in the image used to calculate 4.2 nm, so the true aggregate spacing will be larger.) This behavior in water[51] is attributed to the increased ionic strength of the solution (whether due to added electrolyte or the surfactants themselves, which are also salts) screening electrostatic repulsions between headgroups of adjacent hemimicelles, facilitating their closer packing on the surface. A minimum period is reached when steric interactions prevent closer packing. The absence of any effect of surfactant concentration on hemimicelle period in DESs is thus due to the very high ionic strength of the DES, so that hemimicelles form immediately at their minimum spacing, which is close to the limiting values seen in aqueous systems.

At OCP, the hemimicelle period for SDS in ChCl-Gly (5.2 nm) is slightly greater than for SDS in ChCl-EG (5.0 nm). This is attributed to ChCl-EG being more electrolyte-like than ChCl-Gly;[35] that is, less free cholinium is present in ChCl-Gly. This means the interhemimicelle cholinium concentration is lower in ChCl-Gly, leading to less effective screening of headgroup repulsions and larger interhemimicelle distances and hemimicelle periods.

The effect of applied potential on surface aggregation was probed for ChCl-EG with 25 mM SDS and ChCl-Gly with 10 mM SDS and 2.5 mM CTAB. Experiments were performed at open-circuit potential (OCP), ± 0.5 V and ±0.75 V. The deflection images are presented in the Supporting Information in Figures S1−S3, and the aggregate periods obtained from the images are presented in Table 3.

Table 3. Aggregate Period (nm ± 0.1 nm) as a Function of Potential Determined from AFM Images

	−0.75 V	−0.5 V	OCP	+0.5 V	+0.75 V
ChCl-EG + SDS (25 mM)			5.0 nm	5.5 nm	5.5 nm
ChCl-Gly + SDS (10 mM)			5.2 nm[a]	6.5 nm	6.3 nm
ChCl-Gly + CTAB (2.5 mM)	5.9 nm	6.0 nm	5.5 nm	5.6 nm	5.6 nm

[a]This spacing was determined from an image of ChCl-Gly + SDS (21 mM).

At positive potentials, the SDS adsorbed horizontal monolayer remains intact, with period or deflection scarcely affected. However, at −0.5 V, images of SDS systems were featureless, revealing SDS to be desorbed from the surface. This is attributed to electrostatic repulsion between the negative electrode surface and the dodecyl sulfate anion overcoming attractions between the C_{12} tail and HOPG; SDS is replaced on the surface by the choline cation. In contrast, for ChCl-Gly + 2.5 mM CTAB, surface hemimicelles are present over the entire range of potentials examined. Even at +0.75 V the attraction between the graphite surface and the C_{16} tail of CTAB is strong enough to keep it adsorbed. Calculations show that the free energy of adsorption of Cl^- to graphite at positive potentials is smaller than that of choline under comparable negative potentials,[34] which will also contribute to the retention of the adsorbed surfactant cation.

At positive potentials the aggregate spacing of SDS increases from 5.2 to 5.5 nm in ChCl-EG and from 5.2 to 6.4 nm in ChCl-Gly. A similar increase from 5.5 to 6 nm occurs in CTAB at negative potentials. This effect is attributed to the electrode counterion from the DES being attracted to the electrode surface between aggregates, repelling the like-charged surfactant headgroups and increasing aggregate spacing.

No corresponding change in the period occurs for CTAB at positive potentials. At OCP, the chloride concentration between aggregates is already high because of the positively charged headgroups; therefore, a positive applied potential has minimal effect on interhemimicelle chloride concentration and hence does not affect spacing.

Cyclic voltammograms for a graphite electrode and the pure DESs, ChCl-EG + 25 mM SDS, ChCl-Gly +10 mM SDS, and ChCl-Gly +2.5 mM CTAB are presented in Figure 2. The electrochemical windows of the ChCl-EG and ChCl-Gly are almost identical, but current densities are higher in ChCl-EG,

DOI: 10.1021/acs.jpclett.9b01968
J. Phys. Chem. Lett. XXXX, XXX, XXX−XXX

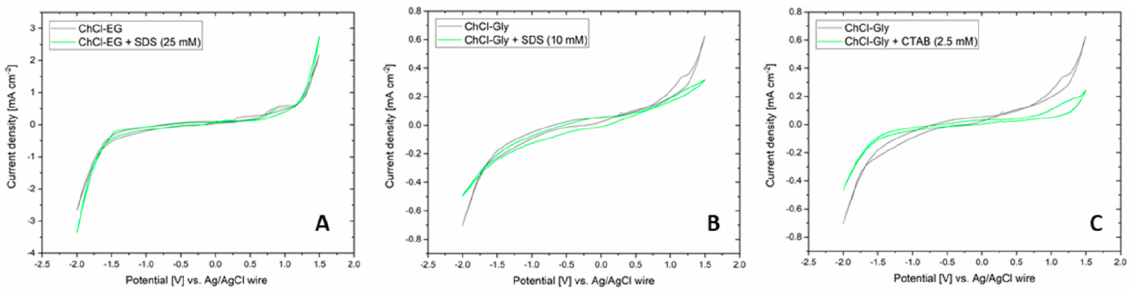

Figure 2. Cyclic voltammograms (green lines) for (A) ChCl-EG + 25 mM SDS, (B) ChCl-Gly +10 mM SDS, and (C) ChCl-Gly +2.5 mM CTAB (2.5 mM). Cyclic voltammograms (black lines) of the pure DES are presented for comparison. Note the *y*-axis scale in panel A is different from that in panels B and C.

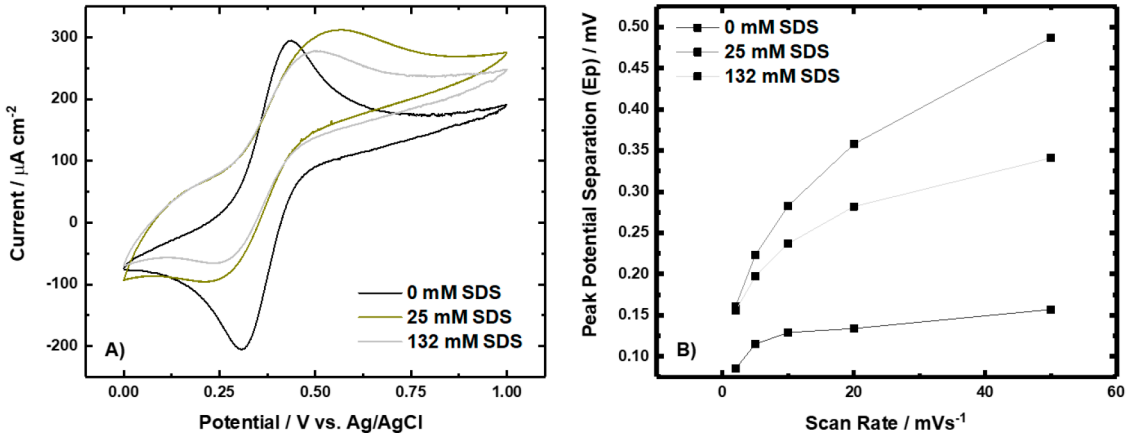

Figure 3. (A) Cyclic voltammetry curves of differing concentrations of SDS at 20 mV/s within a 20 mM $FeCl_2$ ethaline electrolyte at 25 °C on a HOPG electrode and (B) peak-to-peak separation ($E_{pc} - E_{pa}$) vs scan rate in a similar electrolyte.

which is also attributed to ChCl-EG being more electrolyte-like than ChCl-Gly.[35] The voltammogram for ChCl-EG + 25 mM SDS is almost the same as for pure ChCl-EG (Figure 2A). In contrast, for ChCl-Gly +10 mM SDS above 1 V vs Ag/AgCl and below 1.75 V vs Ag/AgCl, current densities are significantly reduced compared to pure ChCl-Gly, but little effect is noted at intermediate potentials. The 2.5 mM CTAB has a much stronger influence on the electrochemical behavior of ChCl-Gly. When CTAB is present, the voltammogram plateau, or capacitive current, at intermediate potentials is closer to horizontal, and the current density at high and low potentials is substantially reduced. This might indicate an enhancement of the electrolyte stability window due to the presence of CTAB at the interface.

Figure 2 reveals CTAB adsorbed as hemimicelles significantly affects the voltammogram for ChCl-Gly, but SDS adsorbed in a tail-to-tail monolayer weakly affects the volatammograms for ChCl-EG/graphite interface and ChCl-Gly/graphite interface. As AFM images as a function of potential revealed that SDS is less strongly bound to the surface than CTAB, the voltammogram data show that the DESs components are able to access the surface in the presence of a relatively weakly bound SDS monolayer, but not for the more strongly bound, hemimicellar, CTAB system. That is, the CTAB aggregates block the electrode surface and inhibit oxidation−reduction processes.

To more carefully probe the impact of horizontal monolayers versus hemimicelles adsorbed to the electrode surface, more sensitive experiments were performed using SDS. Figure 3 probes electron transfer via the redox properties of $FeCl_2$ in ChCl-EG with no surfactant and 25 mM SDS (horizontal monolayer) and 132 mM SDS (hemimicelles). In the absence of SDS, the voltammetry of the $Fe^{III/II}$ redox couple is reversible (Figure 3a) and the peak potential is only slightly affected by the sweep rate because of an uncompensated *iR* artifact (Figure 3b). The same experiments repeated in ChCl-EG with 25 mM SDS caused a slight decrease in the peak current, but the redox potentials of the peaks are moved further apart (Figure 3b). This is due to extended electron transfer occurring across a horizontal monolayer of adsorbed surfactant. A study by Abbott et al. tethered a ferrocene moiety to a CTAB chain in different positions, and it was found that as the redox moiety was further from the electrode the redox behavior became less reversible in aqueous surfactant solution. This was not the case in the absence of unmodified CTAB.[62]

Figure 3a shows that increasing the SDS concentration in ChCl-EG to 132 mM makes the voltammogram even less reversible, and the peak separation increases with increased sweep rate (Figure 3b). This shows the redox-active species are further separated from the electrode surface, consistent with the presence of adsorbed structures.

AFM images reveal striking differences between the structures of the anionic surfactant SDS and cationic surfactant CTAB adsorbed at the interface of ChCl-EG and ChCl-Gly deep eutectics with graphite. SDS only adsorbs as a horizontal monolayer, with surfactants in a tail-to-tail arrangement at around 20 mM, which is far above its critical micelle concentration in both DESs. Only upon increasing the SDS concentration (to 132 mM, almost 15 × CMC in ChCl-EG) are fully formed cylindrical hemimicelles observed. In contrast,

DOI: 10.1021/acs.jpclett.9b01968
J. Phys. Chem. Lett. XXXX, XXX, XXX−XXX

CTAB exhibits a fully developed adsorbed layer of cylindrical hemimicelles on graphite at 2.5 mM, which is only slightly above its CMC in ChCl-Gly (CTAB is insoluble in ChCl-EG). Although the epitaxial monolayer formation on the graphite substrate is always favorable, the subsequent amphiphilic association step is strongly system-dependent.

The SDS and CTAB adsorbed structures also respond very differently to applied potential. In both DESs, SDS is completely desorbed from the interface at negative potentials beyond 0.5 V, while CTAB remains adsorbed at corresponding positive potentials up to +0.75 V. This arises primarily from the stronger attractions between the CTAB hexadecyl tail and graphite compared with the dodecyl tail of SDS, but this is also likely to be affected by the weaker attraction of chloride compared to choline at the polarized graphite surface.

This explains the different effects of these surfactants on the electrochemical behavior of graphite electrodes in DESs. Cyclic voltammograms and electron-transfer experiments show that, for both CTAB and SDS, respectively, adsorbed surfactant hemimicelles influence electrochemical behavior more strongly than a surfactant horizontal monolayer. For CTAB, hemimicelles remain intact across the electrochemical window, forming a more effective barrier at the electrode surface.

Combined, these results show that to effectively modify electrochemical behavior in DESs, care must be taken in the choice of surfactant to ensure that its adsorbed layer forms an effective barrier but also is one that resists desorption when the electrode polarization leads to electrostatic repulsions.

■ ASSOCIATED CONTENT

Supporting Information

The Supporting Information is available free of charge on the ACS Publications website at DOI: 10.1021/acs.jpclett.9b01968.

Experimental section and AFM images (PDF)

■ AUTHOR INFORMATION

Corresponding Author

*E-mail: rob.atkin@uwa.edu.au.

ORCID

Hua Li: 0000-0003-2057-2762

Andrew P. Abbott: 0000-0001-9556-8341

Gregory G. Warr: 0000-0002-6893-1253

Rob Atkin: 0000-0001-8781-7854

Author Contributions

The manuscript was written through contributions of all authors. AFM experiments were performed at UWA by K.H., H.L., and T.T. CV measurements were completed at the University of Leicester by A.P.A.

Notes

The authors declare no competing financial interest.

■ REFERENCES

(1) Abbott, A. P.; Capper, G.; Davies, D. L.; Rasheed, R. K.; Tambyrajah, V. Novel solvent properties of choline chloride/urea mixtures. *Chem. Commun.* **2003**, 70−71.

(2) Meng, X.; Ballerat-Busserolles, K.; Husson, P.; Andanson, J.-M. Impact of water on the melting temperature of urea + choline chloride deep eutectic solvent. *New J. Chem.* **2016**, *40*, 4492−4499.

(3) Hammond, O. S.; Bowron, D. T.; Jackson, A. J.; Arnold, T.; Sanchez-Fernandez, A.; Tsapatsaris, N.; Garcia Sakai, V.; Edler, K. J. Resilience of Malic Acid Natural Deep Eutectic Solvent Nanostructure to Solidification and Hydration. *J. Phys. Chem. B* **2017**, *121*, 7473−7483.

(4) Hammond, O. S.; Bowron, D. T.; Edler, K. J. Liquid structure of the choline chloride-urea deep eutectic solvent (reline) from neutron diffraction and atomistic modelling. *Green Chem.* **2016**, *18*, 2736−2744.

(5) Ashworth, C. R.; Matthews, R. P.; Welton, T.; Hunt, P. A. Doubly ionic hydrogen bond interactions within the choline chloride-urea deep eutectic solvent. *Phys. Chem. Chem. Phys.* **2016**, *18*, 18145−18160.

(6) Araujo, C. F.; Coutinho, J. A. P.; Nolasco, M. M.; Parker, S. F.; Ribeiro-Claro, P. J. A.; Rudić, S.; Soares, B. I. G.; Vaz, P. D. Inelastic neutron scattering study of reline: Shedding light on the hydrogen bonding network of deep eutectic solvents. *Phys. Chem. Chem. Phys.* **2017**, *19*, 17998−18009.

(7) Wei, L.; Zhou, Z.-Y.; Chen, S.-P.; Xu, C.-D.; Su, D.; Schuster, M. E.; Sun, S.-G. Electrochemically shape-controlled synthesis in deep eutectic solvents: Triambic icosahedral platinum nanocrystals with high-index facets and their enhanced catalytic activity. *Chem. Commun.* **2013**, *49*, 11152−11154.

(8) Wei, L.; Fan, Y.-J.; Wang, H.-H.; Tian, N.; Zhou, Z.-Y.; Sun, S.-G. Electrochemically shape-controlled synthesis in deep eutectic solvents of Pt nanoflowers with enhanced activity for ethanol oxidation. *Electrochim. Acta* **2012**, *76*, 468−474.

(9) Goddard, A. J.; Harris, R. C.; Saleem, S.; Azam, M.; Hood, C.; Clark, D.; Satchwell, J.; Ryder, K. S. Electropolishing and electrolytic etching of Ni-based HIP consolidated aerospace forms: A comparison between deep eutectic solvents and aqueous electrolytes. *Trans. Inst. Met. Finish.* **2017**, *95*, 137−146.

(10) Abbott, A. P.; Ryder, K. S.; König, U. Electrofinishing of metals using eutectic based ionic liquids. *Trans. Inst. Met. Finish.* **2008**, *86*, 196−204.

(11) Abbott, A. P.; El Ttaib, K.; Frisch, G.; McKenzie, K. J.; Ryder, K. S. Electrodeposition of copper composites from deep eutectic solvents based on choline chloride. *Phys. Chem. Chem. Phys.* **2009**, *11*, 4269−4277.

(12) Jenkin, G. R.T.; Al-Bassam, A. Z.M.; Harris, R. C.; Abbott, A. P.; Smith, D. J.; Holwell, D. A.; Chapman, R. J.; Stanley, C. J. The application of deep eutectic solvent ionic liquids for environmentally-friendly dissolution and recovery of precious metals. *Miner. Eng.* **2016**, *87*, 18−24.

(13) Karim, W. O.; Abbott, A. P.; Cihangir, S.; Ryder, K. S. Electropolishing of nickel and cobalt in deep eutectic solvents. *Trans. Inst. Met. Finish.* **2018**, *96*, 200−205.

(14) Smith, E. L.; Abbott, A. P.; Ryder, K. S. Deep eutectic solvents (DESs) and their applications. *Chem. Rev.* **2014**, *114*, 11060−11082.

(15) Zhang, Q.; Wang, Q.; Zhang, S.; Lu, X.; Zhang, X. Electrodeposition in Ionic Liquids. *ChemPhysChem* **2016**, *17*, 335−351.

(16) Huang, Y.; Shen, F.; La, J.; Luo, G.; Lai, J.; Liu, C.; Chu, G. Synthesis and Characterization of CuCl Nanoparticles in Deep Eutectic Solvents. *Part. Sci. Technol.* **2013**, *31*, 81−84.

(17) Sirviö, J. A. Fabrication of regenerated cellulose nanoparticles by mechanical disintegration of cellulose after dissolution and regeneration from a deep eutectic solvent. *J. Mater. Chem. A* **2019**, *7*, 755−763.

(18) Chen, S.; Zhang, J.; Wu, T.; Feng, P.; Bu, X. Multiroute synthesis of porous anionic frameworks and size-tunable extraframework organic cation-controlled gas sorption properties. *J. Am. Chem. Soc.* **2009**, *131*, 16027−16029.

(19) Dong, J.-Y.; Lin, W.-H.; Hsu, Y.-J.; Wong, D. S.-H.; Lu, S.-Y. Ultrafast formation of ZnO mesocrystals with excellent photocatalytic activities by a facile Tris-assisted antisolvent process. *CrystEngComm* **2011**, *13*, 6218.

(20) Carriazo, D.; Gutiérrez, M. C.; Ferrer, M. L.; del Monte, F. Resorcinol-Based Deep Eutectic Solvents as Both Carbonaceous Precursors and Templating Agents in the Synthesis of Hierarchical Porous Carbon Monoliths. *Chem. Mater.* **2010**, *22*, 6146−6152.

DOI: 10.1021/acs.jpclett.9b01968
J. Phys. Chem. Lett. XXXX, XXX, XXX−XXX

(21) Hao, G.-P.; Jin, Z.-Y.; Sun, Q.; Zhang, X.-Q.; Zhang, J.-T.; Lu, A.-H. Porous carbon nanosheets with precisely tunable thickness and selective CO2 adsorption properties. *Energy Environ. Sci.* **2013**, *6*, 3740.
(22) Adhikari, L.; Larm, N. E.; Baker, G. A. Argentous Deep Eutectic Solvent Approach for Scaling Up the Production of Colloidal Silver Nanocrystals. *ACS Sustainable Chem. Eng.* **2019**, *7*, 11036−11043.
(23) Elbourne, A.; Sweeney, J.; Webber, G. B.; Wanless, E. J.; Warr, G. G.; Rutland, M. W.; Atkin, R. Adsorbed and near-surface structure of ionic liquids determines nanoscale friction. *Chem. Commun.* **2013**, *49*, 6797−6799.
(24) Endres, F.; Borisenko, N.; El Abedin, S. Z.; Hayes, R.; Atkin, R. The interface ionic liquid(s)/electrode(s): In situSTM and AFM measurements. *Faraday Discuss.* **2012**, *154*, 221−233.
(25) Hayes, R.; Borisenko, N.; Corr, B.; Webber, G. B.; Endres, F.; Atkin, R. Effect of dissolved LiCl on the ionic liquid-Au(111) electrical double layer structure. *Chem. Commun.* **2012**, *48*, 10246−10248.
(26) Hayes, R.; Borisenko, N.; Tam, M. K.; Howlett, P. C.; Endres, F.; Atkin, R. Double Layer Structure of Ionic Liquids at the Au(111) Electrode Interface: An Atomic Force Microscopy Investigation. *J. Phys. Chem. C* **2011**, *115*, 6855−6863.
(27) Li, H.; Endres, F.; Atkin, R. Effect of alkyl chain length and anion species on the interfacial nanostructure of ionic liquids at the Au(111)-ionic liquid interface as a function of potential. *Phys. Chem. Chem. Phys.* **2013**, *15*, 14624−14633.
(28) Maolin, S.; Fuchun, Z.; Guozhong, W.; Haiping, F.; Chunlei, W.; Shimou, C.; Yi, Z.; Jun, H. Ordering layers of bmimPF6 ionic liquid on graphite surfaces: Molecular dynamics simulation. *J. Chem. Phys.* **2008**, *128*, 134504.
(29) McLean, B.; Li, H.; Stefanovic, R.; Wood, R. J.; Webber, G. B.; Ueno, K.; Watanabe, M.; Warr, G. G.; Page, A.; Atkin, R. Nanostructure of Li(G4) TFSI and Li(G4) NO3 solvate ionic liquids at HOPG and Au(111) electrode interfaces as a function of potential. *Phys. Chem. Chem. Phys.* **2015**, *17*, 325−333.
(30) Mezger, M.; Schröder, H.; Reichert, H.; Schramm, S.; Okasinski, J. S.; Schöder, S.; Honkimäki, V.; Deutsch, M.; Ocko, B. M.; Ralston, J.; et al. Molecular layering of fluorinated ionic liquids at a charged sapphire (0001) surface. *Science* **2008**, *322*, 424−428.
(31) Page, A. J.; Elbourne, A.; Stefanovic, R.; Addicoat, M. A.; Warr, G. G.; Voïtchovsky, K.; Atkin, R. 3-Dimensional atomic scale structure of the ionic liquid-graphite interface elucidated by AM-AFM and quantum chemical simulations. *Nanoscale* **2014**, *6*, 8100−8106.
(32) Werzer, O.; Cranston, E. D.; Warr, G. G.; Atkin, R.; Rutland, M. W. Ionic liquid nanotribology: Mica-silica interactions in ethylammonium nitrate. *Phys. Chem. Chem. Phys.* **2012**, *14*, 5147−5152.
(33) Chen, Z.; Ludwig, M.; Warr, G. G.; Atkin, R. Effect of cation alkyl chain length on surface forces and physical properties in deep eutectic solvents. *J. Colloid Interface Sci.* **2017**, *494*, 373−379.
(34) Chen, Z.; McLean, B.; Ludwig, M.; Stefanovic, R.; Warr, G. G.; Webber, G. B.; Page, A. J.; Atkin, R. Nanostructure of Deep Eutectic Solvents at Graphite Electrode Interfaces as a Function of Potential. *J. Phys. Chem. C* **2016**, *120*, 2225−2233.
(35) Hammond, O. S.; Li, H.; Westermann, C.; Al-Murshedi, A. Y. M.; Endres, F.; Abbott, A. P.; Warr, G. G.; Edler, K. J.; Atkin, R. Nanostructure of the deep eutectic solvent/platinum electrode interface as a function of potential and water content. *Nanoscale Horiz* **2019**, *4*, 158−168.
(36) Horn, R. G.; Evans, D. F.; Ninham, B. W. Double-layer and solvation forces measured in a molten salt and its mixtures with water. *J. Phys. Chem.* **1988**, *92*, 3531−3537.
(37) Smith, J. A.; Werzer, O.; Webber, G. B.; Warr, G. G.; Atkin, R. Surprising Particle Stability and Rapid Sedimentation Rates in an Ionic Liquid. *J. Phys. Chem. Lett.* **2010**, *1*, 64−68.
(38) Wang, Z.; Li, H.; Atkin, R.; Priest, C. Influence of Water on the Interfacial Nanostructure and Wetting of RmimNTf2 Ionic Liquids at Mica Surfaces. *Langmuir* **2016**, *32*, 8818−8825.
(39) Abbott, A. P.; Barron, J. C.; Ryder, K. S. Electrolytic deposition of Zn coatings from ionic liquids based on choline chloride. *Trans. Inst. Met. Finish.* **2009**, *87*, 201−207.
(40) Abbott, A. P.; Al-Barzinjy, A. A.; Abbott, P. D.; Frisch, G.; Harris, R. C.; Hartley, J.; Ryder, K. S. Speciation, physical and electrolytic properties of eutectic mixtures based on $CrCl_3{\cdot}6H_2O$ and urea. *Phys. Chem. Chem. Phys.* **2014**, *16*, 9047−9055.
(41) Abbott, A. P.; Ballantyne, A.; Harris, R. C.; Juma, J. A.; Ryder, K. S.; Forrest, G. A Comparative Study of Nickel Electrodeposition Using Deep Eutectic Solvents and Aqueous Solutions. *Electrochim. Acta* **2015**, *176*, 718−726.
(42) Abbott, A. P.; Barron, J. C.; Frisch, G.; Gurman, S.; Ryder, K. S.; Fernando Silva, A. Double layer effects on metal nucleation in deep eutectic solvents. *Phys. Chem. Chem. Phys.* **2011**, *13*, 10224−10231.
(43) Abbott, A. P.; Barron, J. C.; Frisch, G.; Ryder, K. S.; Silva, A. F. The effect of additives on zinc electrodeposition from deep eutectic solvents. *Electrochim. Acta* **2011**, *56*, 5272−5279.
(44) Vittal, R.; Gomathi, H.; Kim, K.-J. Beneficial role of surfactants in electrochemistry and in the modification of electrodes. *Adv. Colloid Interface Sci.* **2006**, *119*, 55−68.
(45) Barron, J. C. *The electrochemistry of Zn in deep eutectic solvents*; Ph.D. Thesis, University of Leicester, Leicester, 2010.
(46) Azam, M. *The electrochemistry of Ag in deep eutectic solvents*; Ph.D. Thesis, University of Leicester, Leicester, 2012.
(47) Abbott, A. P.; Ballantyne, A.; Harris, R. C.; Juma, J. A.; Ryder, K. S. Bright metal coatings from sustainable electrolytes: The effect of molecular additives on electrodeposition of nickel from a deep eutectic solvent. *Phys. Chem. Chem. Phys.* **2017**, *19*, 3219−3231.
(48) Atkin, R.; Craig, V. S. J.; Wanless, E. J.; Biggs, S. Mechanism of cationic surfactant adsorption at the solid−aqueous interface. *Adv. Colloid Interface Sci.* **2003**, *103*, 219−304.
(49) Manne, S.; Cleveland, J. P.; Gaub, H. E.; Stucky, G. D.; Hansma, P. K. Direct Visualization of Surfactant Hemimicelles by Force Microscopy of the Electrical Double Layer. *Langmuir* **1994**, *10*, 4409−4413.
(50) Manne, S.; Gaub, H. E. Molecular Organization of Surfactants at Solid-Liquid Interfaces. *Science* **1995**, *270*, 1480−1482.
(51) Wanless, E. J.; Ducker, W. A. Organization of Sodium Dodecyl Sulfate at the Graphite−Solution Interface. *J. Phys. Chem.* **1996**, *100*, 3207−3214.
(52) Liu, J.-F.; Ducker, W. A. Surface-Induced Phase Behavior of Alkyltrimethylammonium Bromide Surfactants Adsorbed to Mica, Silica, and Graphite. *J. Phys. Chem. B* **1999**, *103*, 8558−8567.
(53) Wanless, E. J.; Ducker, W. A. Weak Influence of Divalent Ions on Anionic Surfactant Surface-Aggregation. *Langmuir* **1997**, *13*, 1463−1474.
(54) Atkin, R.; Warr, G. G. Self-assembly of a nonionic surfactant at the graphite/ionic liquid interface. *J. Am. Chem. Soc.* **2005**, *127*, 11940−11941.
(55) Patrick, H. N.; Warr, G. G.; Manne, S.; Aksay, I. A. Self-Assembly Structures of Nonionic Surfactants at Graphite/Solution Interfaces. *Langmuir* **1997**, *13*, 4349−4356.
(56) Duval, F. P.; Warr, G. G. Shape of tetradecyltrimethylammonium chloride aggregates at liquid/solid interfaces in mixtures of water and formamide. *Chem. Commun.* **2002**, 2268−2269.
(57) Azaga, R. M. M. *Surfactant Aggregation in DESs*; Ph.D. Thesis,University of Leicester, Leicester, 2018.
(58) Sanchez-Fernandez, A.; Arnold, T.; Jackson, A. J.; Fussell, S. L.; Heenan, R. K.; Campbell, R. A.; Edler, K. J. Micellization of alkyltrimethylammonium bromide surfactants in choline chloride:glycerol deep eutectic solvent. *Phys. Chem. Chem. Phys.* **2016**, *18*, 33240−33249.
(59) Okuda, H.; Imae, T.; Ikeda, S. The adsorption of cetyltrimethylammonium bromide on aqueous surfaces of sodium bromide solutions. *Colloids Surf.* **1987**, *27*, 187−200.
(60) Elworthy, P. H.; Mysels, K. J. The surface tension of sodium dodecylsulfate solutions and the phase separation model of micelle formation. *J. Colloid Interface Sci.* **1966**, *21*, 331−347.

DOI: 10.1021/acs.jpclett.9b01968
J. Phys. Chem. Lett. XXXX, XXX, XXX−XXX

(61) Pal, M.; Singh, R. K.; Pandey, S. Evidence of self-aggregation of cationic surfactants in a choline chloride+glycerol deep eutectic solvent. *ChemPhysChem* **2015**, *16*, 2538−2542.
(62) Groszek, A. J. Selective Adsorption at Graphite/Hydrocarbon Interfaces. *Proc. R. Soc. London, Ser. A* **1970**, *314*, 473−498.

DOI: 10.1021/acs.jpclett.9b01968
J. Phys. Chem. Lett. XXXX, XXX, XXX−XXX